High-speed 850 nm VCSELs with 28 GHz modulation bandwidth for short reach communication

Petter Westbergh[*a], Rashid Safaisini[a], Erik Haglund[a], Johan S. Gustavsson[a], Anders Larsson[a], and Andrew Joel[b]

[a]Department of Microtechnology and Nanoscience, Photonics Laboratory, Chalmers University of Technology, Göteborg SE-41296, Sweden;
[b]IQE Europe Ltd., Pascal Close, St. Mellons, Cardiff CF3 0LW, United Kingdom

ABSTRACT

We present results from our new generation of high performance 850 nm oxide confined vertical cavity surface-emitting lasers (VCSELs). With devices optimized for high-speed operation under direct modulation, we achieve record high 3dB modulation bandwidths of 28 GHz for ~4 µm oxide aperture diameter VCSELs, and 27 GHz for devices with a ~7 µm oxide aperture diameter. Combined with a high-speed photoreceiver, the ~7 µm VCSEL enables error-free transmission at data rates up to 47 Gbit/s at room temperature, and up to 40 Gbit/s at 85°C.

Keywords: VCSEL, high speed modulation

1. INTRODUCTION

Vertical cavity surface-emitting laser (VCSEL) based multimode fiber (MMF) links have become key elements in high performance computing systems, data centers, and other short reach datacom networks. These applications are driving the demand for high bandwidth interconnects and it is anticipated that serial bit-rates beyond 40 Gbit/s will be proposed for near future datacom standards. To minimize power consumption, footprint, and cost, it is required that these interconnects operate without active temperature control or cooling. In addition to operation in a room temperature (RT) environment, there is consequently a demand for VCSELs capable of error-free data transmission (defined as a bit-error-rate (BER) $<10^{-12}$) at high bit-rates also under high temperature conditions.

The demand for higher data transmission speed has stimulated research and over the past few years, bit-rates exceeding 40 Gbit/s have been demonstrated for GaAs based VCSELs emitting at 850, 980, and 1090 nm [1-3]. Owing to intrinsic benefits such as lower drive voltages, deeper and more heavily strained quantum wells (QWs), and the possibility of incorporating all binary distributed Bragg reflectors (DBRs) in the structure, the best high temperature performance has so far been achieved for the longer wavelength VCSELs. Error-free transmission at bit-rates up to 38 Gbit/s at temperatures up to 85°C has been demonstrated for 980 nm VCSELs exploiting these design advantages [4]. However, 850 nm is the standard wavelength for MMF based interconnects (high speed MMF such as OM3 and OM4 are optimized for 850 nm) and this is consequently the wavelength of greatest importance for datacom applications. Recently, IBM demonstrated an optical link where a 24 GHz bandwidth 850 nm VCSEL and equalizers were used to enable a serial data rate up to 55 Gbit/s [5]. Currently, this marks the highest achieved bit-rate for a VCSEL based link at RT. At Chalmers, we recently demonstrated a new high-speed 850 nm VCSEL design which enabled us to reach a record high modulation bandwidth of 28 GHz for a ~4 µm oxide aperture diameter VCSEL [6]. With a ~7 µm aperture VCSEL, we were able to demonstrate error-free transmission up to 44 Gbit/s at RT; a bit-rate limit which we partly attributed to our photoreceiver system. Here, we extend the investigatation of the static and dynamic characteristics for our new VCSEL design to include high temperature performance. Using a new high bandwidth photoreceiver, we are able to reach BER$<10^{-12}$ at bit-rates up to 47 Gbit/s at RT and up to 40 Gbit/s at 85°C. This is the highest bit-rate at which error-free transmission has been reported at 85°C, and also the highest bit-rate achieved at RT without using equalizing circuits.

[*] petter.westbergh@chalmers.se; phone +46(0)31 772 1598

2. VCSEL DESIGN

The VCSEL structure presented here (grown by MOCVD at IQE Europe) builds on the high-speed VCSEL design presented in [7] but contains a number of design improvements. The DBR grading and doping schemes have been optimized for low resistance and low free carrier absorption. Compared to our previous design, calculations indicate that the new *p*- and *n*-DBR improve longitudinal conductivity by ~20-30% without increasing optical absorption. These improvements are of benefit for both static and dynamic characteristics as they allow for reaching a higher photon density before thermal rollover sets in, thereby enabling a higher output power and modulation bandwidth.

The active region comprises five strained $In_{0.10}Ga_{0.90}As/Al_{0.37}Ga_{0.63}As$ QWs optimized for high differential gain at 850 nm [8]. A short 0.5-λ cavity is used for improved carrier transport and longitudinal optical confinement [9, 10], properties that both are critical for high-speed characteristics. Our calculations indicate that the longitudinal confinement factor is increased by ~20% for the new cavity layout compared to our previously used 1.5-λ cavity.

As in our previous VCSEL design, the majority of the n-doped bottom DBR contains AlAs as low index material. Since binary AlAs has significantly higher thermal conductivity than ternary AlGaAs, this facilitates heat transport away from the active region and helps delay thermal rollover. The top DBR is *p*-doped and contains two 30 nm thick $Al_{0.98}Ga_{0.02}As$ layers which form the optical and current confining apertures defining the lateral dimensions of the VCSEL cavity. Above these primary oxide layers, four 96% Al-content layers are included in the DBR to reduce the parasitic oxide capacitance which otherwise can limit high-speed performance. The *p*-doped GaAs contact layer is designed as an anti-phase layer which enables the possibility of mode filter integration and post fabrication tuning of the photon lifetime (τ_p) [11, 12]. The optical reflection from the top GaAs/air interface is initially completely out-of-phase with reflections further down in the DBR, resulting in a low reflectivity and a short phonon lifetime. By selectively removing 0-59 nm (59 nm = λ/4) through a shallow surface etch, the photon lifetime can then be tuned between ~0.5 and ~4.1 ps, corresponding to a complete out-of-phase (0 nm) and in-phase (59 nm) reflection, respectively. In the following, we investigate the static and dynamic properties of an unetched ~4 µm oxide aperture VCSEL ($\tau_p \approx 0.5$ ps), and a ~7 µm oxide aperture component with optimized photon lifetime ($\tau_p \approx 1.5$ ps, ~37 nm etch) at RT and at 85°C.
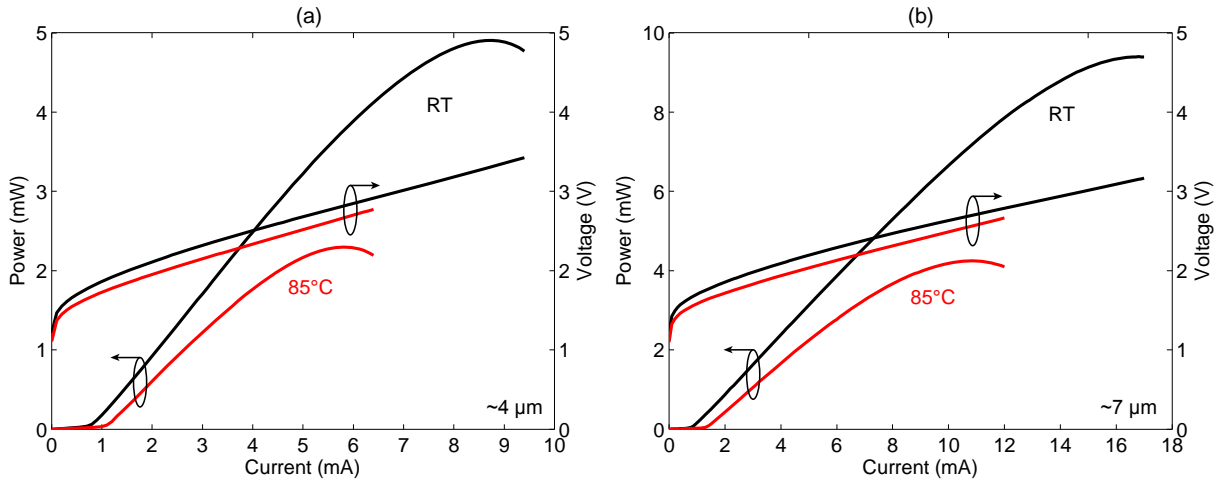
3. STATIC CHARACTERISTICS

Figure 1. Light-current-voltage characteristics for a ~4 µm (a) and a ~7 µm (b) oxide aperture diameter VCSEL at RT and at 85°C.

Figure 1 (a) and (b) shows light-current-voltage characteristics for the ~4 and ~7 µm aperture VCSEL, respectively. The maximum output power drops from 4.9 (9.4) to 2.3 mW (4.3 mW) and the roll-over current from 8.7 (16.8) to 5.8 mA (10.8 mA) when increasing the temperature from RT to 85°C for the ~4 µm (~7 µm) VCSEL. These values are high compared to our previous VCSEL design with similar photon lifetimes, indicating a reduced impact from self-heating as a result from the lower DBR resistance. The differential resistance is ~80 Ω at 10 mA and RT for the ~7 µm VCSEL which roughly corresponds to the reduction in resistance which was expected with the new DBRs. In the new, short cavity design the first 30 nm thick oxide layer is placed at the second null of the optical field outside the separate

confinement heterostructure, leaving a ~110 nm thick section of *p*-doped material between the oxide aperture and the active region. This leads to a lateral current spreading below the oxide aperture which impacts threshold current and internal quantum efficiency (η_i) negatively. The threshold current increases from 0.83 (0.88) at RT to 1.09 mA (1.37 mA) at 85°C for the ~4 µm (~7 µm) VCSEL, values which are approximately twice that of VCSELs with similar photon lifetime and aperture diameter from our previous design. The slope efficiency (SE) is the same for both aperture sizes at 0.75 and 0.62 W/A at RT and 85°C, respectively. This is lower than for comparable VCSELs from our previous design. Best estimates of η_i from measurements of SE as a function of photon lifetime results in numbers around 65-70% for the new VCSEL structure compared to 86% for the previous VCSEL design [7].

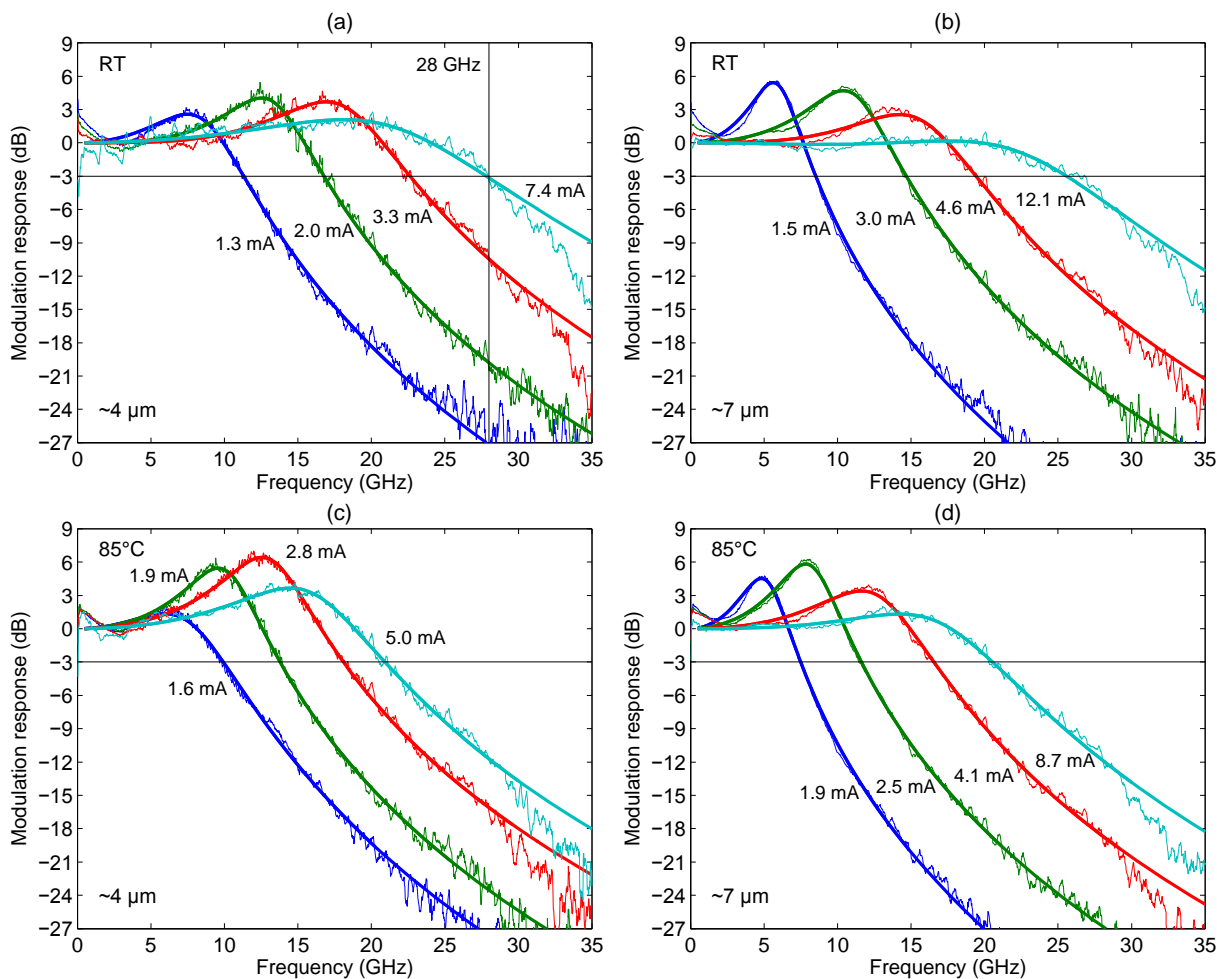## 4. DYNAMIC CHARACTERISTICS

4.1 Modulation response

Figure 2. Measured small signal modulation response for the ~4 µm aperture VCSEL at RT (a) and at 85°C (c) and for the ~7 µm aperture VCSEL at RT (b) and at 85°C (d). In (a), the record high bandwidth of 28 GHz is indicated.

Figure 2 shows the small signal modulation response for the ~4 and ~7 µm aperture VCSELs at RT and 85°C measured with an Anritsu 37397 network analyzer (0.04-65 GHz). The VCSEL under test was probed directly on wafer using a Picoprobe 40A GSG probe. An AR-coated lens package was used to couple the output power to a short OM4 patchcord connected to a New Focus 1481-S-50 25 GHz photodetector. Despite the high threshold currents noted in Section 3, the ~4 µm aperture VCSEL reaches a record high 3dB bandwidth of 28 GHz at RT and 21 GHz at 85°C. The ~7 µm aperture VCSEL reaches a maximum 3dB bandwidth of ~27 GHz at RT and ~21 GHz at 85°C.
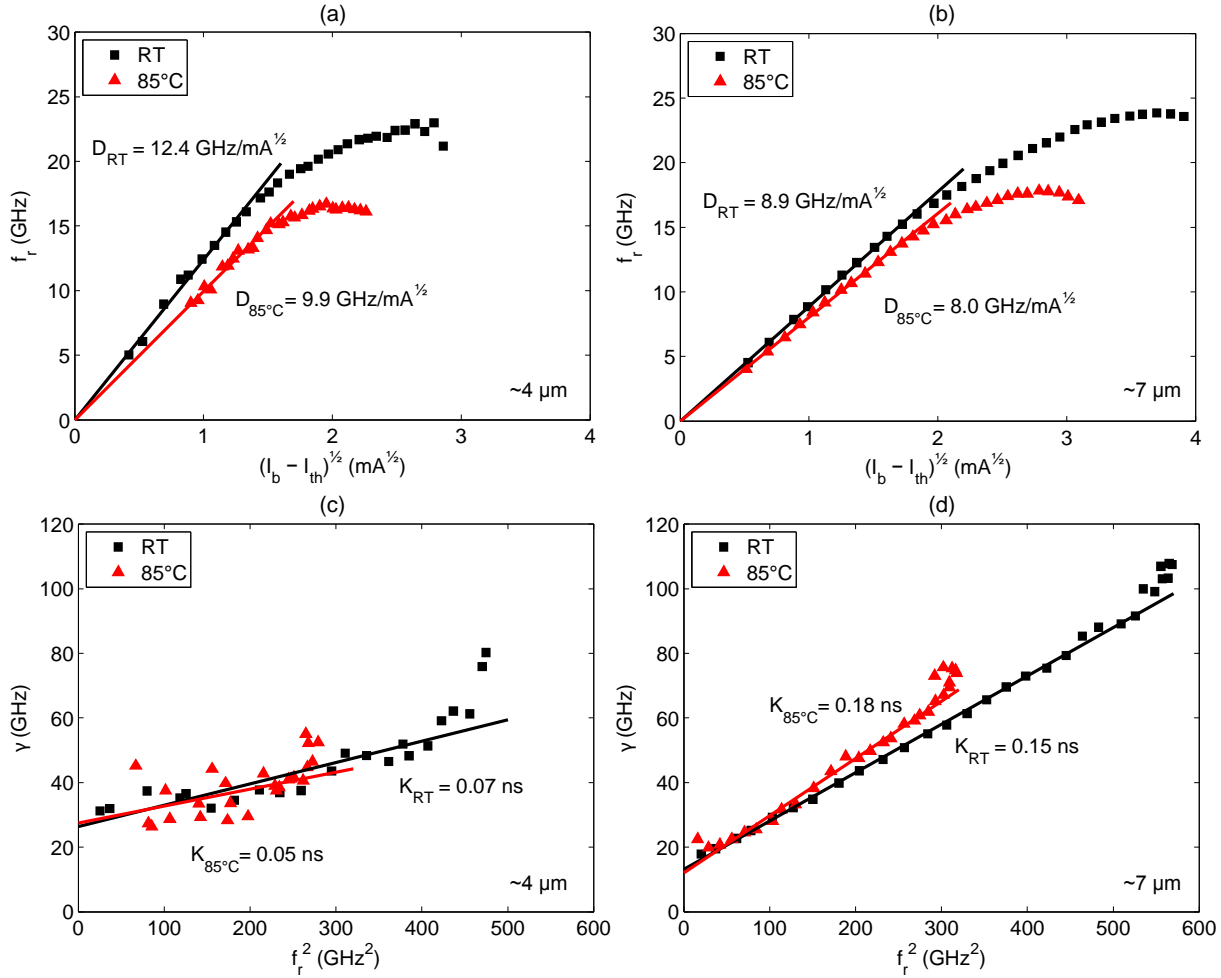
Figure 3. (a) and (b) Resonance frequency vs. square root of bias current above threshold and (c) and (d) damping rate (γ) as a function of resonance frequency squared for the ~4 and ~7 µm aperture diameter VCSELs.

Figures 3 (a) and (b) show the resonance frequency (f_r) as a function of square root of bias current (I_b) above threshold (I_{th}) at both temperatures for the ~4 and ~7 µm aperture VCSEL, respectively. The D-factor is reduced from 12.4 (8.9) to 9.9 GHz/mA$^{\frac{1}{2}}$ (8.0 GHz/mA$^{\frac{1}{2}}$) for the ~4 µm (~7 µm) VCSEL when increasing the temperature to 85°C. These values are higher than for our previous VCSELs with similar aperture size and photon lifetime. An increase of the D-factor is expected when moving to a short cavity because D is proportional to the square root of longitudinal confinement factor (Γ). Since our calculations showed an expected increase of Γ by ~20% (see Section 2), we therefore expect an increase in D-factor of ~10% in the ideal case. However, as mentioned in Section 3, we also observed a reduction of η_i. The full expression for the D-factor can be written as [13]:

$$D = \frac{1}{2\pi} \cdot \sqrt{\frac{\eta_i \Gamma v_g}{q V_a} \cdot \frac{\partial g / \partial n}{\chi}}, \qquad (1)$$

where v_g is the group velocity, V_a the active region volume, $\partial g / \partial n$ the differential gain, and χ is the transport factor. The reduction of η_i thus effectively cancels the expected increase of the D-factor since the product $\eta_i \cdot \Gamma$ remains approximately constant. Instead, we attribute the observed high D-factors and bandwidths to a reduction of the transport factor χ, which results in an increase of the effective differential gain $(\partial g / \partial n) / \chi$ compared to our previous design.

Figures 3 (c) and (d) plot the extracted damping rate (γ) versus resonance frequency at RT and 85°C for the ~4 and ~7 µm aperture VCSEL, respectively. With a photon lifetime at approximately 1.5 ps as a result of the surface etch, the K-factor for the ~7 µm aperture VCSEL is 0.15-0.18 ps. The small aperture component has an intact anti-phase layer on

top and consequently a low photon lifetime (~0.5 ps) which results in low damping and a small *K*-factor between 0.05-0.07 ns. The effect of the low damping on the ~4 µm aperture VCSEL can also be seen in Figure 2, where the modulation response shows signs of peaking near the resonance frequency at the maximum bandwidth. The ~7 µm VCSEL, on the other hand, has a high enough damping to give a flat frequency response without a pronounced resonance peak at the maximum bandwidth. The temperature dependence of the *K*-factor is relatively weak for both components.
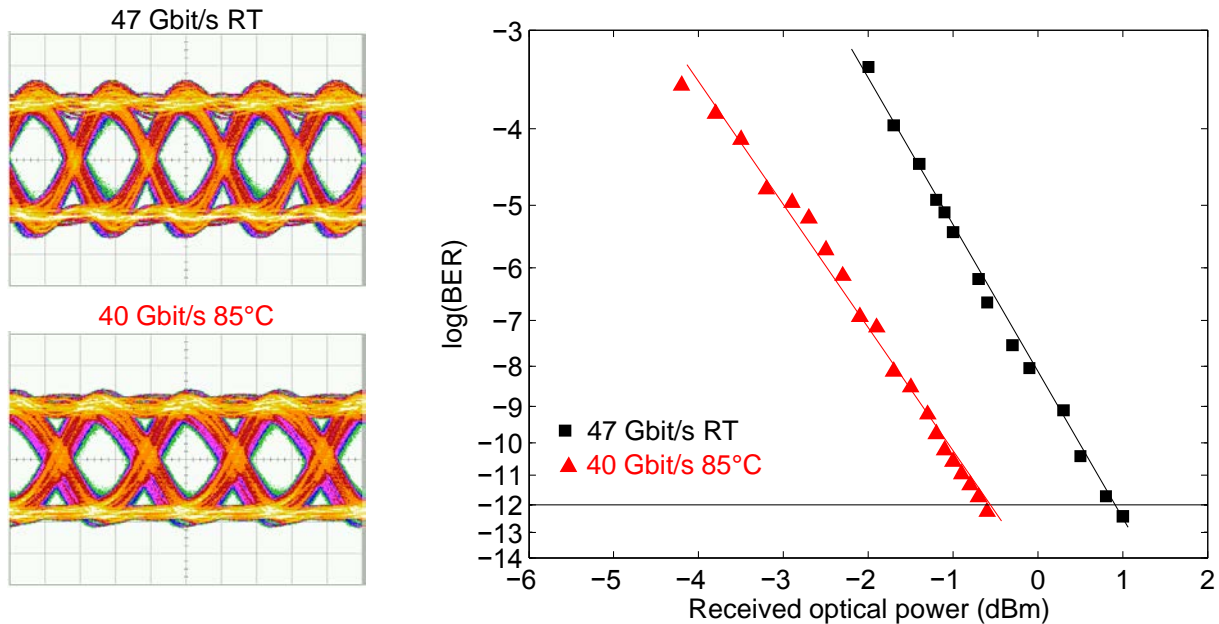
4.2 Large signal modulation

Figure 4. Eye diagrams (scale: 100 mV/div and 10 ps/div) and BER measurement at 47 Gbit/s BTB at RT and at 40 Gbit/s at 85°C for the ~7 µm aperture VCSEL.

In previous experiments, we were able to demonstrate error-free transmission at bit-rates up to 44 Gbit/s with our new generation VCSELs [6]. We partly attributed this bit-rate limit to the optical detection system. Therefore, the measurements are repeated here using a new VI-Systems R40-850 photoreceiver; a prototype receiver consisting of a ≥30 GHz PIN photodetector with an integrated limiting transimpedance amplifier. The experiments were conducted using a 2^7-1 bit non-return-to-zero (NRZ) binary sequence generated by an SHF 12103A bit pattern generator. The drive signal was amplified to 1.0 V_{pp} by an SHF 804 TL amplifier (22dB gain, 55 GHz) in series with 10+3dB electrical attenuators and combined with the DC bias via a bias-T before connecting to the VCSEL. The same probe and output light coupling system as for the modulation response measurements were used here. Before detection, the light was coupled to a JDSU OLA-54 variable optical attenuator to allow for adjusting the level of received optical power for the BER measurements. The electrical signal after the receiver was either connected to an Agilent Infiinum DCA-J 86100C 70 GHz oscilloscope with a precision time base to investigate eye diagrams, or to an SHF 11100B error analyzer to perform BER measurements.

Despite a higher modulation bandwidth, the excessively low damping combined with a high differential resistance (~170 Ω at 7.4 mA) leads to low quality eye diagrams for the ~4 µm VCSEL with a large amount of timing jitter and ringing. The ~7 µm VCSEL only has a marginally lower bandwidth at ~27 GHz, but owing to a flatter frequency response and a better impedance match to the 50 Ω circuits of the experimental setup, the eye diagrams are of significantly better quality. We therefore focus on the ~7 µm aperture VCSEL for these experiments. Figure 4 shows back-to-back (BTB, ~3 m OM4 MMF) eye diagrams and BER data at 47 Gbit/s (RT) and 40 Gbit/s (85°C) for the ~7 µm aperture diameter VCSEL. The eyes are clearly open at both bit-rates and temperatures and BER<10^{-12} is reached in both cases. To the best of our knowledge, these bit-rates mark the highest modulation speeds at which error-free transmission has been demonstrated for any directly modulated VCSEL without using equalizers.

5. CONCLUSIONS

In summary, we present temperature dependent static and dynamic characteristics for our new generation high-speed oxide confined 850 nm VCSELs. The design, which utilizes a 0.5-λ cavity and an improved DBR design, enables maximum modulation bandwidths of 28 GHz at RT for a ~4 µm component, and ~27 GHz at RT for a ~7 µm component. Using a high-speed photoreceiver, we are able to demonstrate error-free data transmission at record speeds of 47 Gbit/s at RT and 40 Gbit/s at 85°C with the ~7 µm oxide aperture diameter VCSEL.

REFERENCES

[1] Westbergh, P., Gustavsson, J.S., Kögel, B., Haglund, Å., Larsson, A., Mutig, A., Nadtochiy, A., Bimberg, D., and Joel, A., "40 Gbit/s error-free operation of oxide-confined 850 nm VCSEL," Electron. Lett. 46(14), 1014-1016 (2010).

[2] Hofmann, W., Moser, P., Wolf, P., Mutig, A., Kroh, M., and Bimberg, D., "44 Gbit/s VCSEL for optical interconnects," Proc. Optical Fiber Communication Conference, paper PDPC5 (2011).

[3] Anan, T., Suzuki, N., Yashiki, K., Fukatsu, K., Hatakeyama, H., Akagawa, T., Tokutome, K, and Tsuji, M., "High-speed InGaAs VCSELs for optical interconnections,". Proc. Int. Symp. on VCSELs and Integrated Photonics, paper E-3 (2007).

[4] Moser, P., Wolf, P., Mutig, A., Larisch, G., Unrau, W., Hofman, W., and Bimberg, D., "85°C error-free operation at 38 Gb/s of oxide-confined 980-nm vertical-cavity surface-emitting lasers," Appl. Phys. Lett. 100(8), 081103-3 (2012).

[5] Kuchta, D. M., Rylyakov, A. V., Schow, C. L., Proesel, J. E., Banks, C., Kocot, C., Graham, L., Johnson, R., Landry, G., Shaw, E., MacInnes, A., and Tatum, J., "A 55Gb/s directly modulated 850nm VCSEL-based optical link," in IEEE Photon. Conf. 2012 (IPC 2012), paper PD 1.5 (2012).

[6] Westbergh, P., Safaisini, R., Haglund, E., Kögel, B., Gustavsson, J. S., Larsson, A., Geen, M., Lawrence, R., and Joel, A., "High-speed 850 nm VCSELs with 28 GHz modulation bandwidth operating error-free up to 44 Gbit/s," Electron. Lett. 48(18), 1145-1147 (2012).

[7] Westbergh, P., Gustavsson, J. S., Kögel, B., Haglund, Å., and Larsson, A., "Impact of photon lifetime on high-speed VCSEL performance," IEEE J. Sel. Top. Quantum Electron. 17(6), 1603-1613 (2011).

[8] Healy, S.B., O'Reilly, E.P., Gustavsson, J.S., Westbergh, P., Haglund, Å., Larsson, A., and Joel, A., "Active Region Design for High-Speed 850-nm VCSELs," IEEE J. Quantum Electron. 46(4), 506-512 (2010).

[9] Nagarajan, R., Ishikawa, M., Fukushima, T., Geels, R.S., and Bowers, J.E., "High speed quantum-well lasers and carrier transport effects," IEEE J. Quantum Electron. 28(10), 1990-2008 (1992).

[10] Mutig, A., and Bimberg, D., "Progress on high-speed 980 nm VCSELs for short-reach optical interconnects," Advances in Optical Technologies, 2011, (1-15) (2011).

[11] Haglund, E., Haglund, Å., Westbergh, P., Gustavsson, J. S., Kögel, B., and Larsson, A., "25 Gbit/s transmission over 500 m multimode fibre using 850 nm VCSEL with integrated mode filter," Electron. Lett. 48(9), 517-517 (2012).

[12] Westbergh, P., Gustavsson, J.S., Kögel, B., Haglund, Å., Larsson, A., and Joel, A., "Speed enhancement of VCSELs by photon lifetime reduction," Electron. Lett. 46(13), 938-940 (2010).

[13] Coldren, L. and Corzine, S., [Diode Lasers and Photonic Integrated Circuits], John Wiley & Sons, Inc., (1995).